JOURNAL OF GEOPHYSICAL RESEARCH: SPACE PHYSICS, VOL. 118, 4253–4269, doi:10.1002/jgra.50397, 2013

Generation of periodic signatures at Saturn through Titan's interaction with the centrifugal interchange instability

R. M. Winglee,[1] A. Kidder,[1] E. Harnett,[1] N. Ifland,[1] C. Paty,[2] and D. Snowden[3]

Received 19 December 2012; revised 11 June 2013; accepted 14 June 2013; published 23 July 2013.

[1] The origin of the periodicities in the radio, plasma, and magnetic fields of Saturn has long been debated. Given the high degree of alignment of Saturn's dipole with its rotation axis, no strong rotational periodicities are expected. However, Cassini data demonstrated the existence of such periodicities not only in Saturn's kilometric radio emissions (SKR) but in the plasma and magnetic field signatures. It is shown that the development of the centrifugal interchange instability that originates from mass loading from the Enceladus torus contains information about the planetary rotation period. However, the planetary period is masked by high-frequency components of the instability. The presence of Titan is shown to damp the high-frequency components and enables the fundamental frequency near the planetary rotation frequency to grow at the expense of the high-frequency components. As a result, the interchange instability is seen to change from one where five to seven large interchange fingers dominate to one where there are about three which cause the modulation of magnetospheric parameters near the planetary period. This modulation includes the movement of the magnetopause, the injection of energetic particles into the inner magnetosphere and the plasma density at high latitudes, both of which control SKR. Controlling factors on the frequency include Titan's drag on the plasma sheet which produces asymmetries between the Northern and Southern Hemispheres, solar wind conditions, and the density of the Enceladus plasma torus. The resultant magnetic perturbations are shown to have similar size and frequency as that seen in Cassini data.

Citation: Winglee, R. M., A. Kidder, E. Harnett, N. Ifland, C. Paty, and D. Snowden (2013), Generation of periodic signatures at Saturn through Titan's interaction with the centrifugal interchange instability, *J. Geophys. Res. Space Physics*, *118*, 4253–4269, doi:10.1002/jgra.50397.

1. Introduction

[2] Saturn's auroral kilometric radiation (SKR) has been used as the primary method to determine its rotational period. The Voyager 1 observations indicated a period of 10 h 39 m 24 s ±7 s [*Desch and Kaiser*, 1981]. With the arrival of Cassini 24 years later, a new inferred period of 10 h 45 min 45 s ±36 s was determined [*Gurnett et al*., 2005; *Kurth et al*., 2008]. This difference in the inferred period cannot be due to changes in planet's rotation, and therefore must be due to plasma/magnetic processes within the Kronian magnetosphere that control the generation of SKR.

[3] Periodicities are seen in many of the key characteristics of the Kronian magnetosphere including the magnetic field [*Espinosa and Dougherty*, 2000; *Espinosa et al*., 2003; *Giampieri et al*., 2006; *Jackman and Arridge*, 2011], low energy plasma [*Gurnett et al*., 2007; *Burch et al*., 2008], energetic charged particles [*Carbary et al*., 2007], and in energetic neutral atoms [*Paranicas et al*., 2005; *Carbary et al*., 2008]. Even the position of the magnetopause appears to have the same periodicity [*Clarke et al*., 2010].

[4] Understanding the source of these periodicities is very difficult because Saturn's magnetic field is closely aligned with the planet's rotation axis. As such, the spin of such a highly aligned dipole alone is not expected to produce the observed periodicities by itself. Further confusion is brought about by the recent observation that the SKR emission consists of two separate components with different rotation modulation rates, one from the north (at about 10.6 h) and one from the south auroral region (at about 10.8 h) [*Gurnett et al*., 2009]. These two rates appeared to converge about 7 months after Saturn's equinox in 2009. *Carbary et al*. [2009] have also noted the presence of the dual period in the energetic electron data.

[5] *Gurnett et al*. [2009] posited two theories for such long-term variation: one, that instabilities in Saturn's dynamo produce rotating magnetic anomalies, and two, that Saturn's magnetosphere slips with respect to the dipole, and this slippage rate is controlled by field-aligned

Additional supporting information may be found in the online version of this article.

[1]Department of Earth and Space Science, University of Washington, Seattle, Washington, USA.
[2]School of Earth and Atmospheric Science, Georgia Institute of Technology, Atlanta, Georgia, USA.
[3]Lunar and Planetary Laboratory, University of Arizona, Tucson, Arizona, USA.

Corresponding author: R. M. Winglee, Department of Earth and Space Science, University of Washington, Box 351310, Seattle, WA 98195-1310, USA. (winglee@ess.washington.edu)

2169-9380/13/10.1002/jgra.50397

currents. *Burch et al*. [2008] proposed that a localized interchange-driven plasma outflow produces magnetic reconnection at the observed periodicity, which then results in the injection of energetic particles that produces the periodicity in the observed SKR emissions and other plasma properties. This was similar to a mechanism proposed for the Jovian magnetosphere [*Kivelson and Southwood*, 2005].

[6] *Jia et al*. [2012] have proposed that the source of the periodicities originates from localized vertical structures in the ionosphere near 70° latitude generated by the coupling between the atmosphere and the ionosphere. Difference vortices in the northern and southern hemisphere were used by *Jia and Kivelson* [2012] to produce the apparent difference in the periodicities seen between these hemispheres. Observations confirming the presence of these localized vortices have yet to be made. These works also use a single fluid MHD model where all the plasma irrespective of its origin are assumed to be O^+ so that the presence of the interchange instability is not fully incorporated in the model since the instability requires the presence of both light and heavy ion species.

[7] Detailed multifluid simulations have been used to examine the development of the interchange instability [*Kidder et al*., 2009]. Outward convection of heavy ion plasma from Enceladus leads to a centrifugal interchange instability. This instability causes heavy ions that originate from Enceladus to move outward while hotter but more tenuous solar wind plasma is drawn inward, leading to the formation of discrete interchanging fingers of plasma. The present simulations as described in section 2 are essentially the same as that used in prior work of *Kidder et al*. [2009] and *Winglee et al*. [2009], but the density at the inner boundary has been increased to the in-line with the more recent Cassini observations of *Kellett et al*. [2010]. Reexamination of the interchange instability in section 3 in terms of periodicity demonstrates that while the planetary period is embedded in the interchange instability, the dominate frequencies are at a harmonic of the planetary frequency with the fundamental having a lower power than the second harmonic. Thus, the embedding of a clear periodicity by the interchange instability alone as proposed by *Burch et al*. [2008] is not explicitly seen in a Saturn only model.

[8] Recent multiscale simulations by *Winglee et al*. [2009] that include Titan within the Kronian magnetosphere have shown that Titan can cause the disruption of the interchange fingers. At the same time, the interaction causes flapping of Titan's ion tail. However, these initial simulations were limited in duration to a few hours due to the disparate spatial scales between Titan's induced magnetosphere and the Kronian magnetosphere.

[9] With the faster computers that are now available, we have now run the multiscale/multifluid simulations (section 4) over a much longer timescale (over 100 h including both Saturn and Titan). Analysis of these results shows that Titan's interaction with the interchange fingers damps the higher frequency components of the interchange instability and causes a strong fundamental (near the planetary rotation frequency) component to develop. This change occurs because Titan and its ion tail provide a drag force on the rotating magnetospheric plasma such that smaller finger instabilities coalesce into larger and less frequent fingers. Larger fingers move beyond Titan's orbit, but can be disrupted when they interact with Titans induced magnetosphere. During such an interaction, there is partial reflection of energy back into the inner magnetosphere associated with the flapping of Titan's ion tail. This flapping was seen in initial Saturn/Titan simulations [*Winglee et al*., 2009] with the feedback on the interchange finger only becoming evident in the longer duration simulations presented here. This leads to modified interchange fingers that are larger but less frequent than seen in the Saturn only simulations. These modified interchange fingers can modulate the position of the magnetopause [cf. *Snowden et al*., 2011a, 2011b] and lead to the reduction of plasma density at high latitudes when the magnetosphere is expanding. Such density reductions favor the generation of SKR and in this way the planetary period can be embedded into the SKR signal (section 5). These results reinforce the earlier finding by *Menietti et al*. [2007] who indicated that Titan may modify SKR. Differences between the northern and southern hemispheres are also demonstrated with the summer hemisphere experiencing the strongest drag from Titan and having a slightly longer period than the northern hemisphere consistent with Cassini observations.

[10] Since the interchange instability develops from mass loading from Enceladus, we also demonstrate that the frequency can be shifted depending on the prevailing conditions at the Enceladus torus (section 6). Increasing the density in the inner magnetosphere as well as stronger solar wind forcing is known to increase the frequency of the interchange instability [*Kidder et al*., 2009]. In the presence of drag from Titan, this leads to a decrease in the apparent fundamental period of the system with an increase of a factor of 4 in density producing a shift of about 1 h in the apparent period of the system.

[11] In section 7, we compare the model results with magnetometer data from Cassini revolutions 23 and 32. It is shown that the model is able to produce magnetic perturbations of comparable magnitude and frequency as the observations. The model also is able to explain the high-frequency component and nonsinusoidal features in the Cassini data which suggests that the proposed mechanism is at work within the Kronian magnetosphere. A summary of results is given in section 8. Our results show that the impact of a moon with an ionosphere that can support ion outflow can have much more impact on the global dynamics of the planetary magnetosphere than previously thought. A full description of these fast rotating planetary magnetospheres needs to include not only magnetospheric/ionospheric coupling but also coupling between the planetary magnetosphere and the induced magnetosphere around the planet's moons.

2. Model

2.1. Multifluid Equations

[12] The multifluid equations are exactly the same as in *Kidder et al*. [2009] and *Winglee et al*. [2009] and incorporate ion skin depth effects in Ohm's law and ion cyclotron terms in the momentum equation that can lead to the differential acceleration of different ion species. The dynamics of each plasma component is described

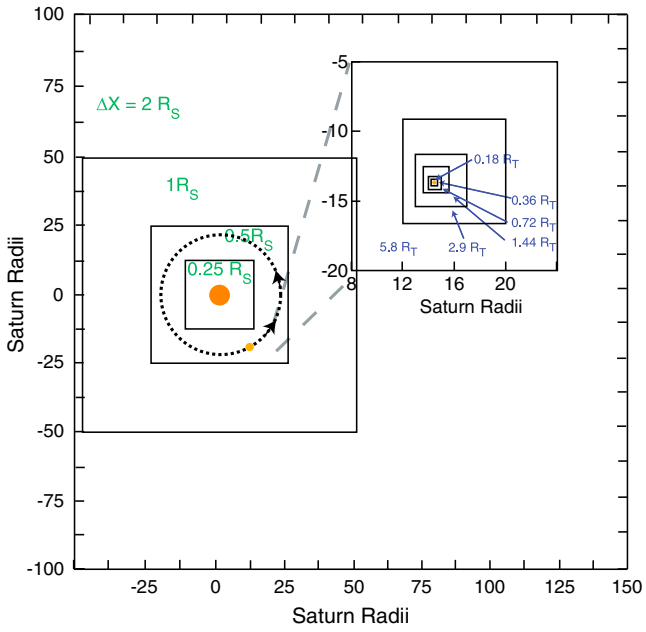

Figure 1. Nested-grid system that incorporates both Saturn's magnetosphere and Titan's induced magnetosphere. Only the inner boxes are shown for clarity. Numbers inside boxes indicate the resolution. In order to maintain high resolution gridding around Titan, the refinement grid is moved with the orbital motion of Titan.

by conservation equations for mass, momentum, and pressure given by

$$\frac{\partial \rho_\alpha}{\partial t} + \nabla\cdot(\rho_\alpha \boldsymbol{V}_\alpha) = 0 \tag{1}$$

$$\rho_\alpha \frac{\mathrm{d}\boldsymbol{V}_\alpha}{\mathrm{d}t} = q_\alpha n_\alpha(\boldsymbol{E} + \boldsymbol{V}_\alpha \times \boldsymbol{B}) - \nabla P_\alpha - \left(\frac{GM}{R^2}\right)\rho_\alpha \vec{\boldsymbol{r}} \tag{2}$$

$$\frac{\partial P_\alpha}{\partial t} = -\gamma\nabla\cdot(P_\alpha \boldsymbol{V}_\alpha) + (\gamma - 1)\boldsymbol{V}_\alpha\cdot\nabla P_\alpha \tag{3}$$

where the subscript α denotes the ion and electron components that constitute the plasma and γ is the adiabatic index equal to 5/3 for 3-D simulations. In hybrid codes, and in the multifluid code, one makes the assumption that the electrons are a fluid and have sufficiently high mobility along the field lines such that they are approximately in steady state (i.e., $\mathrm{d}v_e/\mathrm{d}t = 0$) or in drift motion. This assumption removes high-frequency plasma and electron waves and enables the momentum equation for the electrons to be reduced to

$$\boldsymbol{E} + \boldsymbol{V}_e \times \boldsymbol{B} + \frac{\nabla P_e}{en_e} = 0 \tag{4}$$

[13] The electron dynamics are completed by assuming quasi-neutrality and applying the definitions for current and electron pressure. For a single component plasma, one obtains

$$N_e = N_i, \quad \boldsymbol{V}_e = \boldsymbol{V}_i - \frac{\boldsymbol{J}}{eN_e}, \quad \boldsymbol{J} = \frac{1}{\mu_0}\nabla \times \boldsymbol{B} \tag{5}$$

$$\frac{\partial P_e}{\partial t} = -\gamma\nabla\cdot(P_e \boldsymbol{V}_e) + (\gamma - 1)\boldsymbol{V}_e\cdot\nabla P_e \tag{6}$$

[14] In the presence of multiple ion populations, (5) becomes

$$n_e = \sum_i n_i, \quad \boldsymbol{V}_e = \sum_i \frac{n_i}{n_e}\boldsymbol{V}_i - \frac{\boldsymbol{J}}{en_e}, \quad \boldsymbol{J} = \frac{1}{\mu_0}\nabla \times \boldsymbol{B} \tag{7}$$

[15] Substitution of (9) into (4) yields a modified Ohm's law of

$$\boldsymbol{E} = -\sum_i \frac{n_i}{n_e}\boldsymbol{V}_i \times \boldsymbol{B} + \frac{\boldsymbol{J} \times \boldsymbol{B}}{en_e} - \frac{1}{en_e}\nabla P_e + \eta(x)\boldsymbol{J} \tag{8}$$

[16] The first term in (8), when assuming a single ion species, collapses into the ideal Ohm's law. The last term, $\eta(x)J$, is added only to allow for finite conductivity in the ionospheres of Saturn and Titan. Collisions beyond this region are assumed to be negligible. No anomalous resistivity is included in the code.

[17] The second and third terms in (8) are the Hall and Grad P_e corrections and become significant when the ion skin depth becomes comparable to the scale length of gradients. Ion cyclotron terms can be derived from the full momentum equation and the modified Ohm's law given by (8). Thus, the above equations incorporate key particle effects provided that the actual particle distributions modeled are approximately Maxwellian.

[18] The evolution of the magnetic field is determined by the induction equation

$$\frac{\partial \boldsymbol{B}}{\partial t} + \nabla \times \boldsymbol{E} = 0 \tag{9}$$

where the electric field is given by the modified Ohm's law in (8). Note also that each ion species contributes to the electric field in (8) which produces coupling between the species. These equations are more complicated than the MHD equations and no simple conservative form of the equations exist because of the coupling. Nevertheless, convergent solutions are easily obtained using standard techniques. The above equations are solved using a second order Runge-Kutta method.

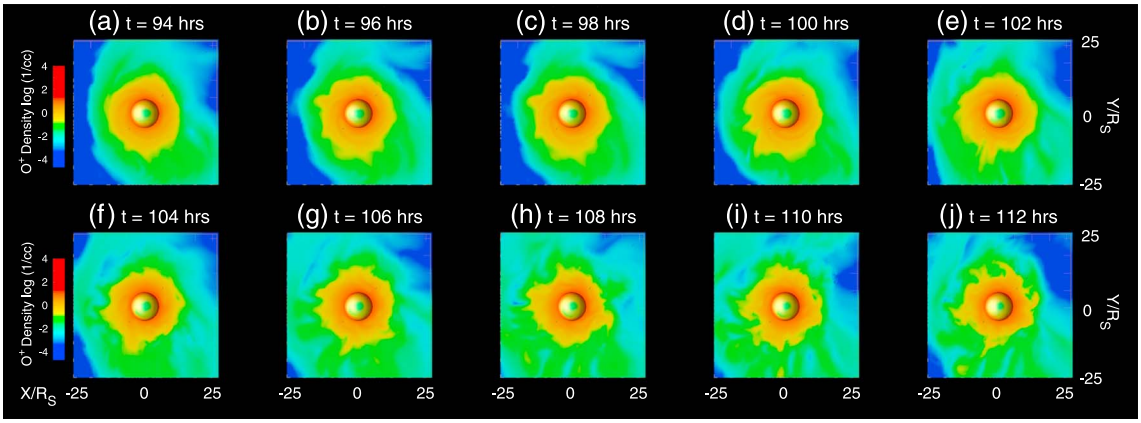

Figure 2. The equatorial O^+ plasma density spaced 2 h apart with the top row showing plasma properties for one period and the bottom row approximately one planetary period later. The sphere in the center has a radius twice as large as the inner boundary so that properties of the plasma can be mapped onto its surface to indicate process occurring at high latitudes. The interchange fingers are seen as high density regions extending out in radial distance. It is seen that a fixed observer will see a similar feature passing between consecutive periods though other features will be seen during a planetary period.

2.2. Grid System

[19] The Kronian magnetosphere is modeled through a series of five staggered/nested grid systems. The inner box has a grid spacing of 0.25 R_S and an inner boundary of 2.25 R_S and extends out to ±12 R_S in x and y directions and ±6 R_S in the z direction. The grid spacing in each successive box increases by a factor of two with the final box spanning 700 R_S down tail and ±400 R_S in the y direction and ±180 R_S in the z direction with a resolution of 8 R_S. A schematic for the four innermost boxes is shown in Figure 1. The runs with Saturn only (i.e., no Titan) have been run out 250 h in real time under various solar wind conditions (described in the next section).

[20] For the runs that include Titan, we include a refinement grid (also shown in Figure 1) that overlies the Kronian grid system with increasing resolution in successive grids to resolve the plasma processes around Titan. This refinement grid consists of six additional staggered boxes that provide coverage of ±2 R_S in each direction with the gridding spacing decreasing by a factor of 0.5 between successive boxes. In the innermost grid, the grid spacing is 900 km around Titan with the inner boundary set at the base of the exosphere at 1.5 Titan radii.

[21] This grid is similar to that used in *Winglee et al.* [2009] which provided the first study of Titan's induced magnetosphere with the Kronian magnetosphere. In this earlier study both Titan and the refinement grid were assumed to be stationary; the runs were performed for ~20 h, and then restarted with different solar wind conditions. In the present work both Titan and the refinement grid are moved at Titan's orbital speed.

[22] Titan is inserted at about 40 h into the Saturn only run. The simulations are then run for an additional 20 h enabling Titan's induced ionosphere to come into equilibrium with the Kronian magnetosphere. After this period, the simulations are continued in excess of 100 h to test for periodicities. It should be noted that these runs are four times slower than the Saturn only runs so that variations due to solar wind conditions are not considered here.

2.3. Model Plasma Parameters

[23] The inner boundary conditions for our simulations are similar to those implemented in *Kidder et al.* [2009] where they studied the development of the centrifugal interchange cycle driven by plasma sourced from Enceladus and its neutral cloud except that the inner density is higher to bring it in line with recent Cassini observations [*Kellett et al.*, 2010]. The model includes one electron component (whose dynamics is determined by equations (5)–(8)) and three ion components (controlled by equations (1)–(3)): (a) protons which can originate from the solar wind and/or the planetary/moon ionosphere; (b) moderately heavy ions such as O^+, N^+, OH^+, H_2O^+, or CH_4^+ (with an assumed overall mass of 16 amu), hereafter referred to as the O^+ group; and (c) the heavy ions such as N_2^+ and O_2^+ (with an assumed mass of 32 amu), hereafter referred to as the heavy ion group (Hvy^+). The latter two ions species have either the Enceladus torus or Titan as their source. The Enceladus ion source is incorporated in the model by placing an ion torus with a density of 50 cm^{-3} O^+ ions at Enceladus' orbit and 5 cm^{-3} Hvy^+ ions. The plasma torus is initialized on field lines that enclose Enceladus' L shell at 4 ± 0.5. This yields an extended torus that would be associated with ionization of neutrals well away from Enceladus. The density derived from this initialization is held fixed at the points where the torus intersects the inner boundary.

[24] An H^+ ionosphere is assumed at the inner boundary of 2.25 R_S, representing Saturn's ionosphere, and the inner boundary of the simulations. At latitudes above $L = 4$, the ionospheric density is held constant at a value of 5 cm^{-3} and decreases to 1.25 cm^{-3} at the equator.

[25] The boundary conditions for Titan are held fixed for the duration of the simulations and are the same as in *Winglee et al.* [2009]. Specifically, the density of O^+ and Hvy^+ is set to 400 particles/cm^3, with the proton density set at 200 particles/cm^3. The temperatures of Saturn and Titan's ionospheres are assumed to be low at ~1 eV. A Cartesian coordinate system is such that Saturn's rotation axis is in the z direction and the negative x axis is pointed to the Sun,

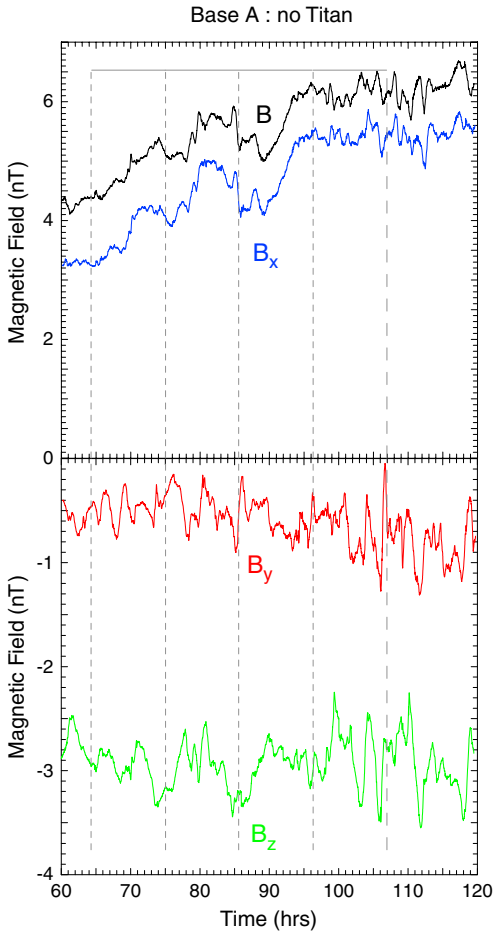

Figure 3. The time history of the magnetic field at (20,0,0) R_S in the tail. All components show some evidence of the planetary period though it is strongest in B_z and there are strong high frequency components present particularly in B_y.

with the Sun being in the *x-z* plane though it is below the equatorial plane of Saturn. Titan is started at [0, −20, 0] R_S, i.e., in at dusk.

[26] We model southern summer conditions when Saturn's rotation axis is tilted out of the ecliptic plane, the solar wind is incident at an upward angle of 28° with a velocity of 500 km/s and a density of 0.06 cm^{-3}. For these conditions, the solar wind dynamic pressure is sufficiently low that Titan's orbit always remains at least 2 R_S inside the magnetopause.

3. Saturn Only Simulations

[27] The evolution of the equatorial O^+ density in the absence of Titan is shown in Figure 2. The panels in the figure are arranged so that the rows show images through successive rotations. The columns are arranged so that they represent approximately the same phase of the rotation. It is seen that the density profile at any given time has several radial extensions. These features are produced by the interchange instability, and the detailed evolution of individual interchange fingers has been as detailed by *Kidder et al*. [2009] and is not repeated here. It is sufficient to note that at any particular time, there are approximately five to seven interchange fingers present. The fingers are largest between noon and premidnight. There is a tendency for some of the mass of the fingers to be ejected down the tail so that in the postmidnight to dawn sector, the fingers are relatively short.

[28] Looking down the columns, it is seen that there is a high probability that if an interchange finger is observed in the first rotation, an interchange finger will be observed one rotation later. It should be noted that it is not necessarily the same finger that is observed one rotation later. The fact that the interchange instability involves an azimuthal wave mode means that rotational information is embedded in the characteristics of the developing instability so that some periodic behavior is expected.

[29] Halfway during the 20 h period shown, the solar wind density is reduced by 20% which produces some outward motion of the magnetopause. Despite this change, the mode number for the interchange fingers remains between about five and seven. This result suggests that while the solar wind may control the size of the Kronian magnetosphere, it is not the dominant controlling factor in setting the mode number for the interchange instability. As such, the interchange

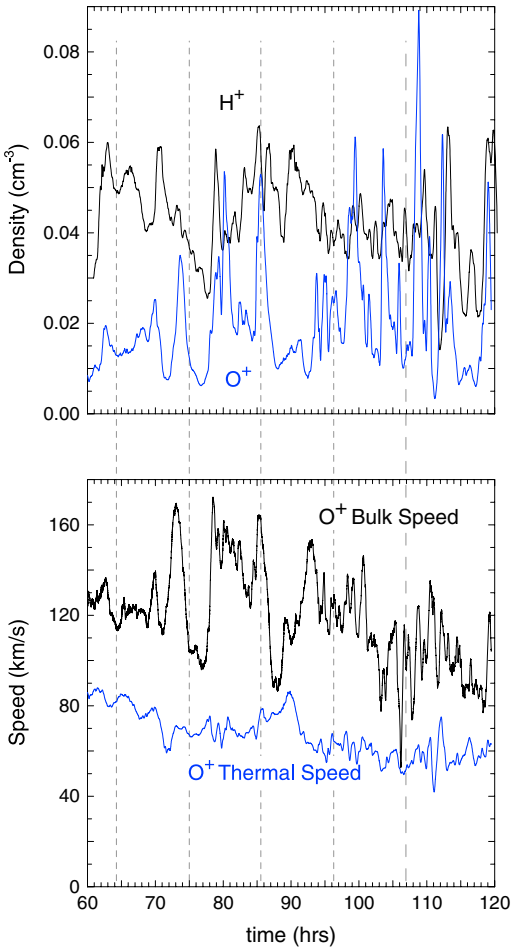

Figure 4. The time history of the plasma properties at the same observing position in Figure 3. The density variations have a strong high-frequency component which makes any correlation with the planetary period difficult to discern. The plasma bulk speed though does some evidence of variations at the planetary period.

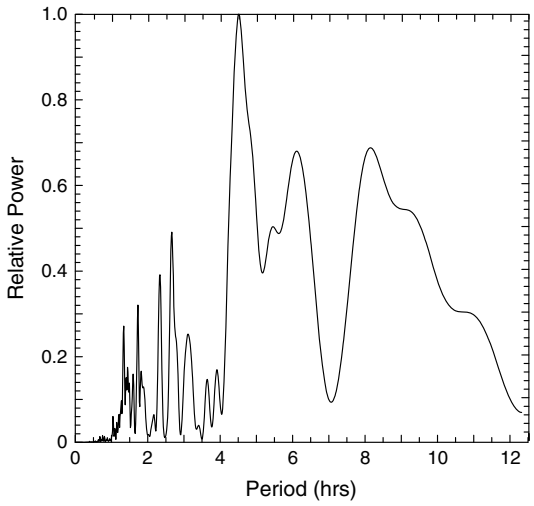

Figure 5. Fourier transform of the magnetic field in Figure 3. The dominant peak is at about 4.5 h with a weaker broad peak between about 8 and 10 h.

fingers retain some information on the rotational processes that control their formation.

[30] In order to derive the exact frequency response, the magnetic field and plasma parameters were sampled at several locations around the magnetosphere. As an example of the response that would be seen along Titan's orbit, we show only a representative example taken at (20,0,0) R_S down the tail in Figure 3. Figure 3 (top) shows the time evolution of the magnitude of magnetic field (B) and the B_x component over 60 h. The lower panel shows the evolution of B_y and B_z with the dashed lines showing the rotation period. Both B and B_x have a DC response to the decrease in the solar wind dynamic pressure. The DC component reflects the motion of the observing point away from the center of the current sheet. The presence of any single feature that is repeated at the planetary period is difficult to discern in the data.

[31] For the B_z, the larger minima tend to line up at approximately the rotation period, but there is clear evidence of a higher frequency component. This higher frequency component is particularly strong in the B_y component. These high-frequency components are due to the fact that there is in fact many small interchange fingers present that sweep passed an observing point at a higher rate than the rotation period.

[32] The corresponding evolution of the light and heavy ion densities are shown in the top panel of Figure 4. The bottom panel shows the O^+ bulk speed and thermal speed (the speeds for H^+ have a similar time dependence and are not shown). Similar to the magnetic field, there are strong high-frequency components though there are features that have the rotational period embedded within them including the deep minimum in O^+ density and bulk speed occurring near the rotational period. It is for this reason that the sampling done in Figure 2 appears to show periodic reappearance of features though there are many additional features moving passed an observing point at any particular time. Indeed, on reexamining the interchange fingers originally identified in *Kidder et al.* [2009], we found that the same conclusion can be reach in that there are multiple fingers present but at a fixed

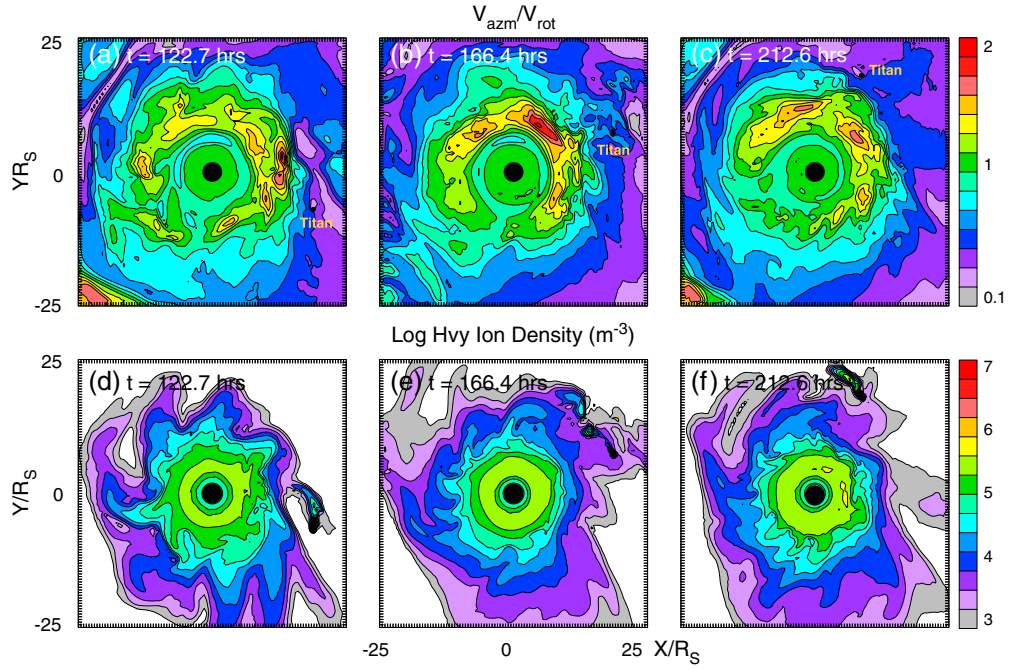

Figure 6. The (top) azimuthal velocity in the equatorial plane and the (bottom) Hvy^+ ion density to indicate the positions of the interchange fingers and the position of Titan and its ion tail are shown. Corotation dominates until ~7 R_S. This region is followed by a section where a two-cell convection pattern is imposed on the rotation field such that the convection speeds are enhanced on the dawnside and reduced on the duskside. Over a few hours in local time about Titan, there is a suppression of the convection velocities around Titan and an increase in the speeds needs the breakdown of the corotation velocities.

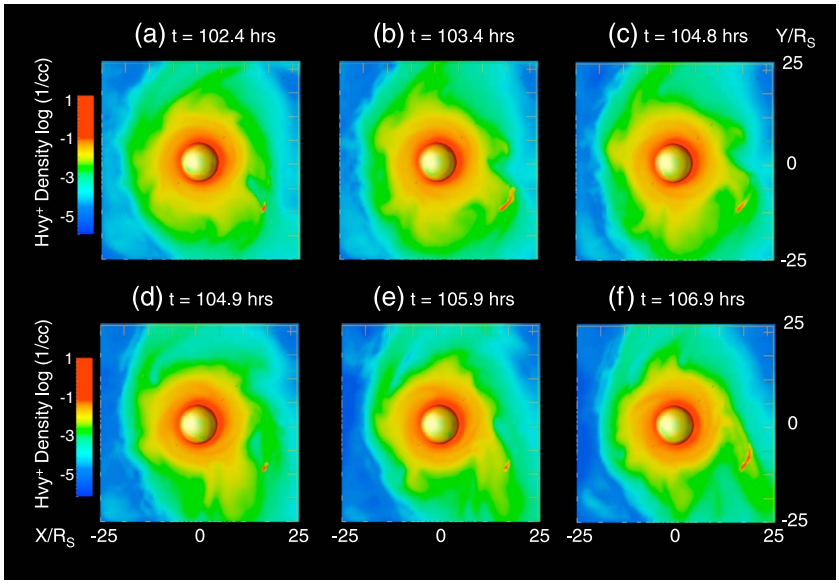

Figure 7. Equatorial Hvy^+ plasma density with Titan included. Merging of interchange fingers is seen to occur producing larger but fewer interchange fingers rotating around the Kronian magnetosphere.

point if one sees an interchange finger then there is a high chance an interchange finger will be seen one rotation period later irrespective of local time.

[33] In order to quantify the exact frequencies present, a Fourier transform (FT) of the profiles in Figures 3 and 4 was performed. All profiles gave similar results, so that for an illustrative example, FT of the magnetic field is shown in Figure 5. It is seen that there are several peaks to the spectrum with the dominant mode at having a period between 4.5 and 6 h. This period corresponds to the time interval for large (or fully developed) interchange fingers. The smaller less well-developed interchange fingers have even short periods that are present between 1.5 and 3 h. There is also a broad peak around the planetary period, but it is not the dominant component, and the width of the peak is much wider than the well-defined planetary period of SKR. These results reinforce the conclusion that information on the rotational period is contained within the interchange fingers, but in the absence of Titan, the dominant mode is near to the second harmonic and not at the fundamental, though there is some power at the fundamental. In other words, the interchange instability while having some rotational information embedded in it, the instability by itself is unable to produce a dominant mode at the planetary period that could account of the observed periodicity in SKR.

4. Saturn/Titan Simulations

[34] As noted in *Winglee et al*. [2009], the presence of Titan can affect the development of the interchange fingers, and conversely the interchange fingers can modify the properties of Titan's ion tail. In other words, there is coupling between the two entities, and as shown in the following, this coupling is important in identifying a strong fundamental component in the plasma properties that is missing from the Saturn only simulations of the previous section.

[35] The large range influence of Titan is illustrated in Figure 6, which shows the azimuthal velocity divide by the corotation velocity (top panels) and the Hvy^+ ion density (bottom panels) from which Titan's positions and the interchange fingers can easily be discerned. The azimuthal velocity is seen to be approximately corotation out to about 7 R_S. Beyond this distance, there is an increase of the azimuthal velocity particularly on the dawn side out to about 11 R_S, after which there is full departure from corotation. This local maximum in speed is due to the penetration of a two-cell convection pattern which on the dawnside enhances the rotational flows which are directed toward the Sun. On the duskside, the convection flow is also toward the Sun which in the opposite direction of the rotational flows. In addition to this effect, there is an enhancement in the inner magnetosphere of the azimuthal velocity of about 10–20% within ±3 h of local time of Titan. This enhancement is Titan induced since it moves in local time with Titan. At the same time, there is a reduction in the azimuthal velocity at radial distances a few R_S about Titan and this reduction extends a few hours in local time.

[36] The above effect of Titan on the rotational velocity can be understood as follows. Titan produces a drag on the magnetosphere since it is moving at an orbital speed instead of corotation. Because the region is sub-Alfvénic, the drag effect can propagate both upstream and downstream by a few R_S. Because this drag produces a restriction to the inherent magnetospheric flows, and some of this flow is forced to remain inside of Titan's orbit at small radial distances than they would have in the absence of Titan. Conversation of flux and angular momentum means that the plasma in the inner magnetosphere speeds up while the plasma near Titan slows down.

[37] The effect on the interchange instability is shown in Figure 7 which shows the O^+ density in the equatorial plane with a cadence of about 1 h. At t = 102.4 h, Titan is past the first of a set of three interchange fingers. Its ion tail at this time is relatively short. By t = 103.4 h, the last of three fingers

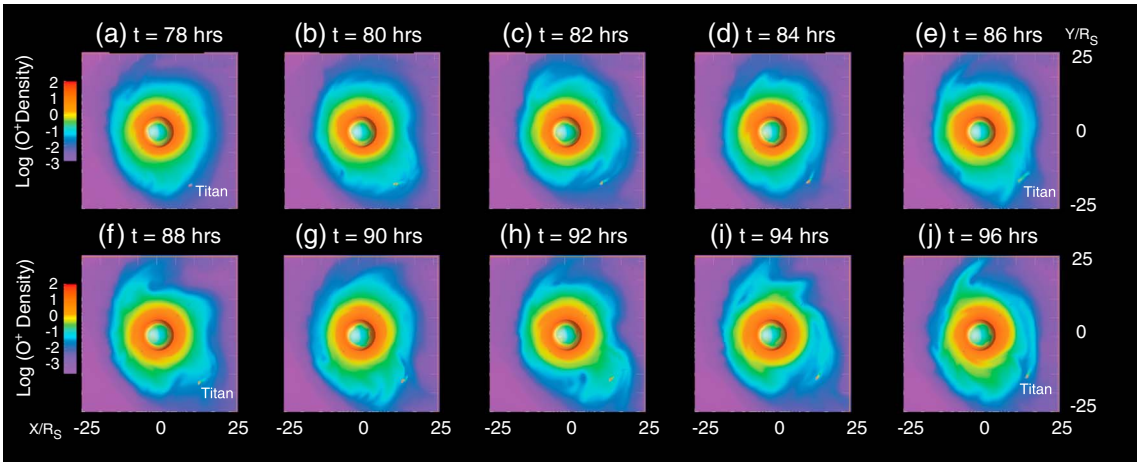

Figure 8. The equatorial O^+ density over two successive rotations similar to the Saturn only simulations shown in Figure 2. Due to the presence of Titan there are fewer large-scale interchange fingers present.

has caught up to the middle fingers; and by 104.8 h, the middle and last interchange fingers have essentially merged into a larger single finger. These process repeats itself in the bottom frames where again there are two distinct interchange fingers approaching Titan; while after they interact with Titan, there is a single large finger and Titan's tail is temporarily enhanced.

[38] As a result of this Titan induced merging of fingers, there are only three to four large fingers present as opposed to the five to seven fingers present in the Saturn only simulations of the previous section. This effect is further illustrated in Figure 8, which shows the evolution of the O^+ density over two rotation periods. Through either of the periods, there are a reduced number of large interchange fingers. If one looks down the columns, it seen that irrespective of local time, if there is a large finger present in one rotation period then it is highly likely that a large finger will also be seen in the next rotation period, similar to the Saturn only simulations. Again, this result does not suggest that it is the same finger that is being observed, only that one is present each rotation. The fact that there are fewer large fingers present though means that the dominant frequency is reduced.

[39] While we have demonstrated that there is modulation of the Kronian system by the coupling of Titan and the interaction fingers, we still have to prove that it leads to conditions that are conducive to SKR and that the dominant period is related to the planetary period. Let us first demonstrate that the presence of modified interchange fingers is conductive to the generation of SKR, and then examine a Fourier analysis of particle and magnetic signatures.

[40] The modification of the interchange fingers modifies the injection of energetic particles from the middle magnetosphere. This effect is illustrated by the temperature profiles shown in Figure 9. At first time shown (Figure 9a), there is an energetic particle injection event where particles from the middle magnetosphere are seen moving sunward on the dawn flank. Some of these particles continue to move toward the magnetopause and flow back down the tail. However, a

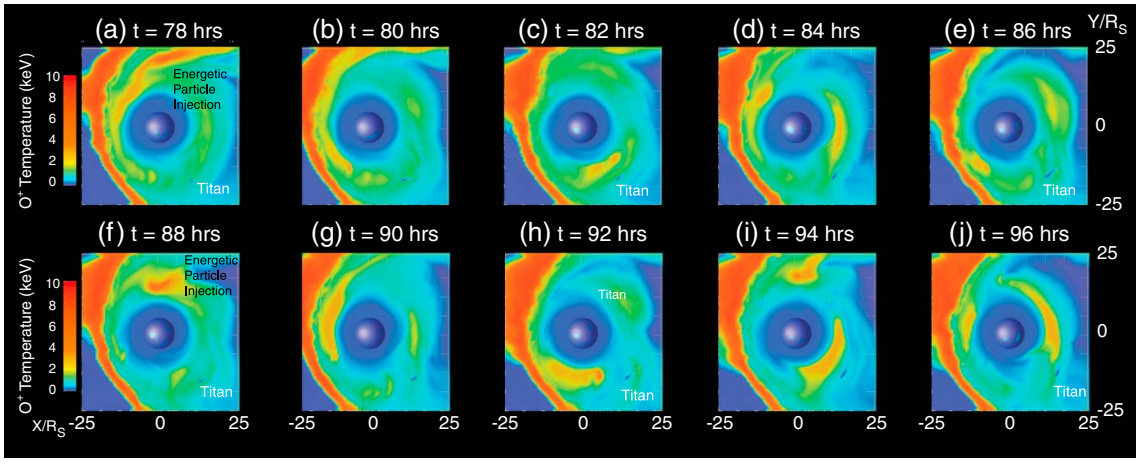

Figure 9. The equatorial O^+ temperature at all the same times in Figure 8. An injection of energetic particles is seen at the start of both Saturn rotations. The temperature profile of these injections seems to be modified as they pass inside of Titan's orbit. Looking down the columns, one sees that if there is an energetic population present in the first rotation and there is a high probability that an energetic population is seen in the next rotation, irrespective of local time.

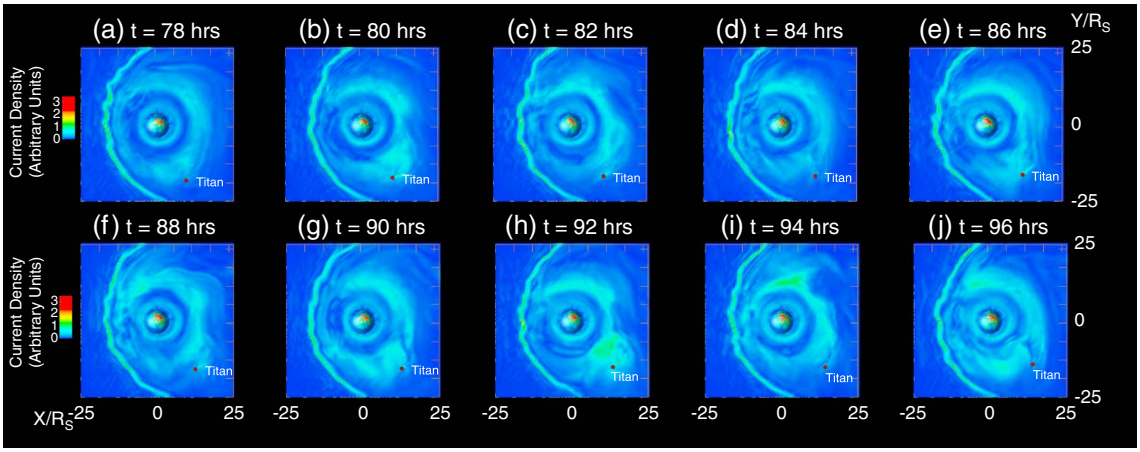

Figure 10. The equatorial current density corresponding to Figures 8 and 9. Excluding the magnetopause currents, the strongest currents tend to be in the dawnside except for intensification as the energetic particles pass inside of Titan indicating that Titan has substantial impact on the dynamics of the Kronian magnetosphere.

portion of these particles is seen to enter into the inner magnetosphere (Figure 9b) and passes inside of Titan (Figure 9c). As they do so, further energization is seen and this plasma then moves into the nightside. At the same time, new energetic particle populations occur in the prenoon sector (Figure 9d). The process is then seen to repeat itself in the next cycle. Thus, a fixed observer in the inner magnetosphere will see an energetic particle population pass by at the rotation period. However, there are actually two energetic particle populations present at any given time. The acceleration of these discrete populations is enhanced by the presence of Titan, and the acceleration is very much more disperse in space so that a discrete Titan footprint in the Kronian ionosphere would be difficult to discern.

[41] The associated evolution of the equatorial currents is shown in Figure 10. The magnetopause currents that are evident on the dayside and show some rippling are due to a Kelvin-Helmholtz-like instability. The injection itself (Figure 10a) is associated with only a weak enhancement in the equatorial currents. However, as the energetic particles move toward Titan (Figures 10b and 10c), there is enhancement of current across several R_S in the local time sector occupied by Titan. As the energetic particles move past Titan, a reduction in the currents about Titan occurs. When the energetic particles reach the predawn sector, there is a resurgence in the current density (Figure 10f). This cycle is seen to repeat with a new intensification of current about Titan in Figure 10g. A depression of current associated with Titan's ion tail near midnight is also seen at this time. Further intensification is seen in Figure 10h, which is then followed by intensification of current in the dawn sector in Figures 10i and 10j. It is interesting to note that the currents in the second cycle are more intense than those in the first rotation of their injection. These results show that Titan does in fact have a significant impact on the plasma properties well beyond its immediate vicinity, and these effects include those of the energetic particles and currents that can map to high latitudes.

[42] The other important effect is that the modified interchange fingers lead to modification of the density at high latitudes. The interchange fingers alter the position of the magnetopause [*Snowden et al.*, 2011a, 2011b]. This effect

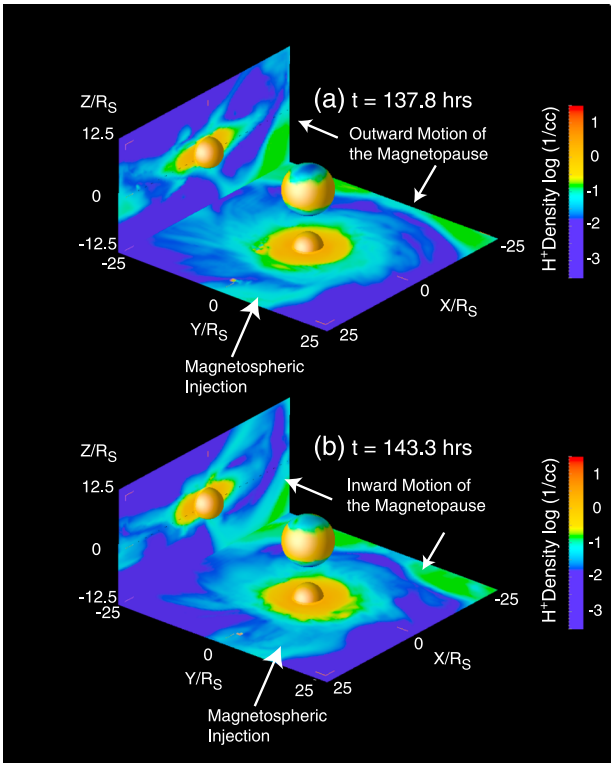

Figure 11. Cutaway views of the H^+ density on the noon-midnight meridian and equatorial planes. The sphere in the center has a radius of twice the inner boundary. At both times, there is an injection of energetic particles occurring in the postmidnight sector. The first time shown the magnetopause has been pushed outward by a modified interchange finger, and the density at high latitudes is at its lowest. At 4.5 h later, the magnetopause, especially on the dawnside, is seen moving inward and there are increased densities at high latitudes including the cusp and high latitude boundary layers.

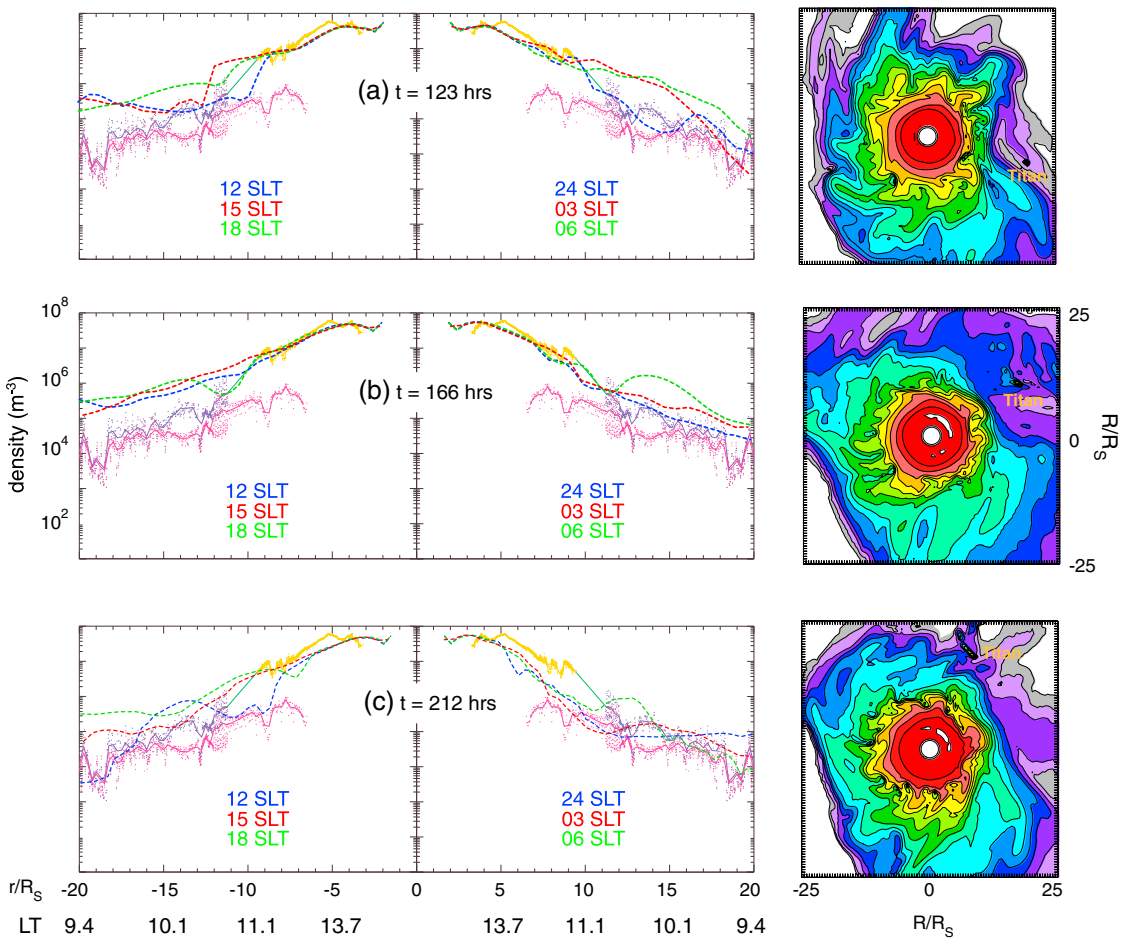

Figure 12. Comparison of the model densities (dashed lines) relative to the Cassini observations (dots and yellow lines) from *Kellett et al*. [2010]. The Cassini observations have been reflected so that comparisons on both the dayside and nightside can be made. There are substantial variations in the model such that the average value is above that of the observations but at the times when the model density is lowest there is general agreement between observations and model. The differences in profiles are attributed to variations produced by the movement of the magnetopause as well as Titan's interaction with the Kronian magnetosphere.

is demonstrated in Figure 11 which shows a 3-D view of the proton density. The equatorial density is shown in the bottom segment and the density in the noon-midnight meridian is shown to the right. The density at 4 R_S is projected onto the sphere in the middle. In the first time frame shown, an injection of hot magnetospheric protons is starting to occur and the magnetopause is being pushed outward by an interchange finger. The corresponding density of H^+ at high latitudes is very low with the density over the polar cap less than 10^{-2} cm^{-3}. As this interchange finger rotates around to the duskside, the magnetopause moves inward and there are substantially more protons in the high altitude regions with a thicker cusp in both hemisphere. Some of the equatorial H^+ is now seen at high latitudes in the noon-midnight meridian. The density over the polar cap as seen on the center sphere is seen to be several times higher as well.

[43] Since SKR is dependent on both the presence of energetic particles and low plasma density, it is seen that the interchange instability as modified by Titan is able to produce modulations in both these properties. Animations of the plasma density, temperature, and currents are included in the supporting information.

5. Time Variations in the Kronian Magnetosphere

[44] Figure 12 shows some of the variations seen in the plasma density in both time and space within the inner magnetosphere. The left column show radial cuts of the equatorial O^+ density (i.e., Kronian plasma only) through the noon-midnight meridian, the dawn-dusk terminator, and a 45° cut from postnoon to predawn. The dayside profiles ions observed by Cassini [*Kellett et al*., 2010] are overlaid. In order to obtain an estimate of the densities in the nightside, we have reflected the Cassini profile. Contours in the equatorial density are shown to the right. Three different times are shown to give some indication of temporal versus spatial differences. It is seen that within the inner magnetosphere at <8 R_S, the model densities are comparable to the observed density and these profiles are approximately symmetric. Beyond 8 R_S, the nightside density on average tends to be

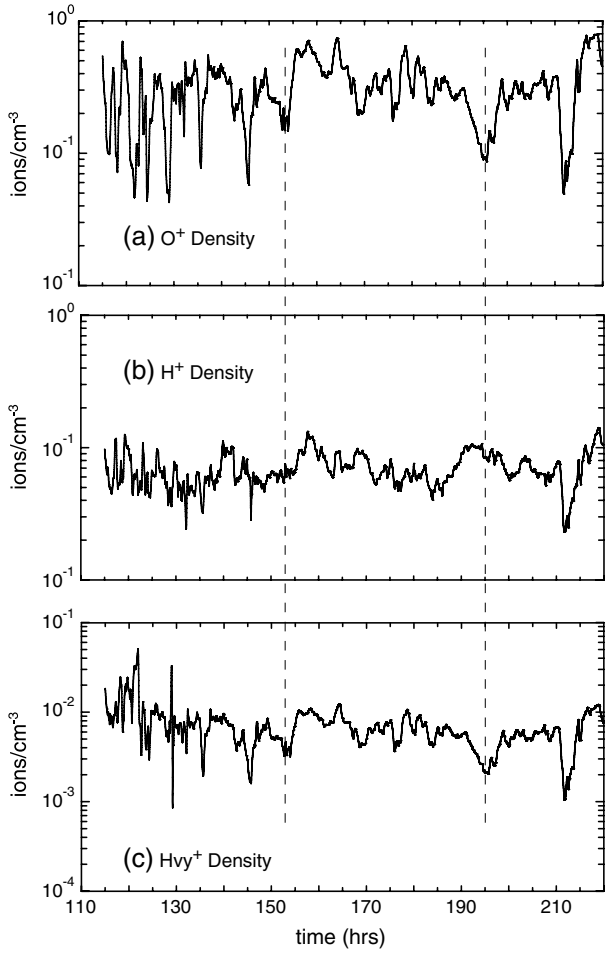

Figure 13. Time variations in the plasma density at a fixed point at $R = (20,0,3)$ R_S. There is the appearance of a long timescale periodicity of about 40–50 h that is superposed on the shorter timescale fluctuations near the second harmonic and/or the planetary rotation period. Because of the relative strength of both long period variations relative to those near the planetary period, a clean spectrum cannot be obtained for these parameters.

lower than the dayside density except when a large interchange finger is present. In the latter case, the density can jump by a factor of 5–10. The densities at $t = 166$ h (middle column) tend to be highest and the magnetosphere at its largest extend. At the other two times when the magnetopause is closer in to Saturn, the densities are reduced and comparable to that observed by Cassini. It should also be noted that since the model densities are taken through the center of the plasma sheet, the derived densities should be on average higher than the Cassini data since the latter need not be exactly centrally located.

[45] The relatively high density at $t = 166$ h is part of a longer period oscillation which is shown Figure 13. This figure shows the time evolution of the ion species at 20 R_S down the tail and +3 R_S in Z. The latter displacement places the point near the center of the current sheet when the shape of the bowl shape of the magnetosphere is taken into account. All of the density profiles show modulation at timescales comparable to or shorter than the planetary rotation, with modulations of the order of a factor of 5 to 10. There is though a longer timescale of the order of 40 to 50 h where there is a slow decrease by a factor of 2–3 in O^+ and Hvy^+ densities. A larger than average injection event (seen in the H^+ density profiles as indicated by the dashed lines) is followed by or is coincident with an increase in the O^+ and Hvy^+ densities. We have yet to fully analyze the source of this longer period modulation since much longer runs have to be performed to fully establish the presence of any persistent trend. The point is that the changes in the density profiles in Figure 12 are due to both short-term and long-term processes.

[46] The presence of the planetary period embedded in the plasma properties is most easily seen in Figures 14a–14d, which shows the flux per unit area of Kronian O^+ and H^+ that is incident on Titan as it moves through its orbit. These fluxes are obtained by integrating the particle fluxes over a 0.2 R_S cube about Titan. The most striking feature is that the incident fluxes are strongly modulated with the dominant frequency being at about half the planetary period when Titan is in the premidnight sector. This periodicity declines when Titan is in the midnight to postmidnight sector, and the periodicity reasserts itself when Titan reaches the predawn/dawn sector with both high- and low-frequency components present. The dropout near midnight is due to the truncation of the interchange fingers as large fingers tend to go from the dusk sector down the tail as opposed to turning the corner to maintain rotation with the planet. The Fourier transform of the O^+ flux time history shows strong peaks at approximately 6 and 11 h.

[47] The H^+ ions which include the hot magnetospheric plasma do not show this drop out. Moreover, the spectrum has its strongest peak near the planetary period. In comparing Figure 5 with Figure 14, we see that by including Titan we have gone from a system where the second harmonic is dominant to a system where the fundamental is the dominant feature for the injection of hot magnetospheric plasma. Moreover, as the integration period is increased from 60–240 h (dashed lines) to 60–340 h (solid lines), the relative strength of the second harmonic decreases relative to the fundamental.

[48] The resultant total flux of Hvy^+ from Titan is shown in Figures 14e and 14f. It is seen that the outflow from Titan also has strong modulations at the fundamental and second harmonic. In addition to these components, the outflow has substantially stronger high-frequency components so that while many of the interchange fingers are truncated, interchange perturbations are still reaching Titan such that its outflow appears to be modified down to the faster frequencies of the interchange instability. Similar to the spectra of the inflowing material, the high-frequency components appear weaker as the integration period is increased.

[49] As noted in the previous section, Titan's influence extends well beyond its orbit. To demonstrate this further, Figure 15 shows the time history and spectral analysis of the magnetic field at 10 R_S on the dawnside. Figures 15a and 15b (Figures 15c and 15d) show the results at 2 R_S below (above) the equator illustrating the response of the southern (northern) hemispheres. It is seen that the responses for the two hemispheres are not identical. This result is expected since the solar wind is incident on the southern hemisphere and Titan is therefore below the centerline of the bowl shape

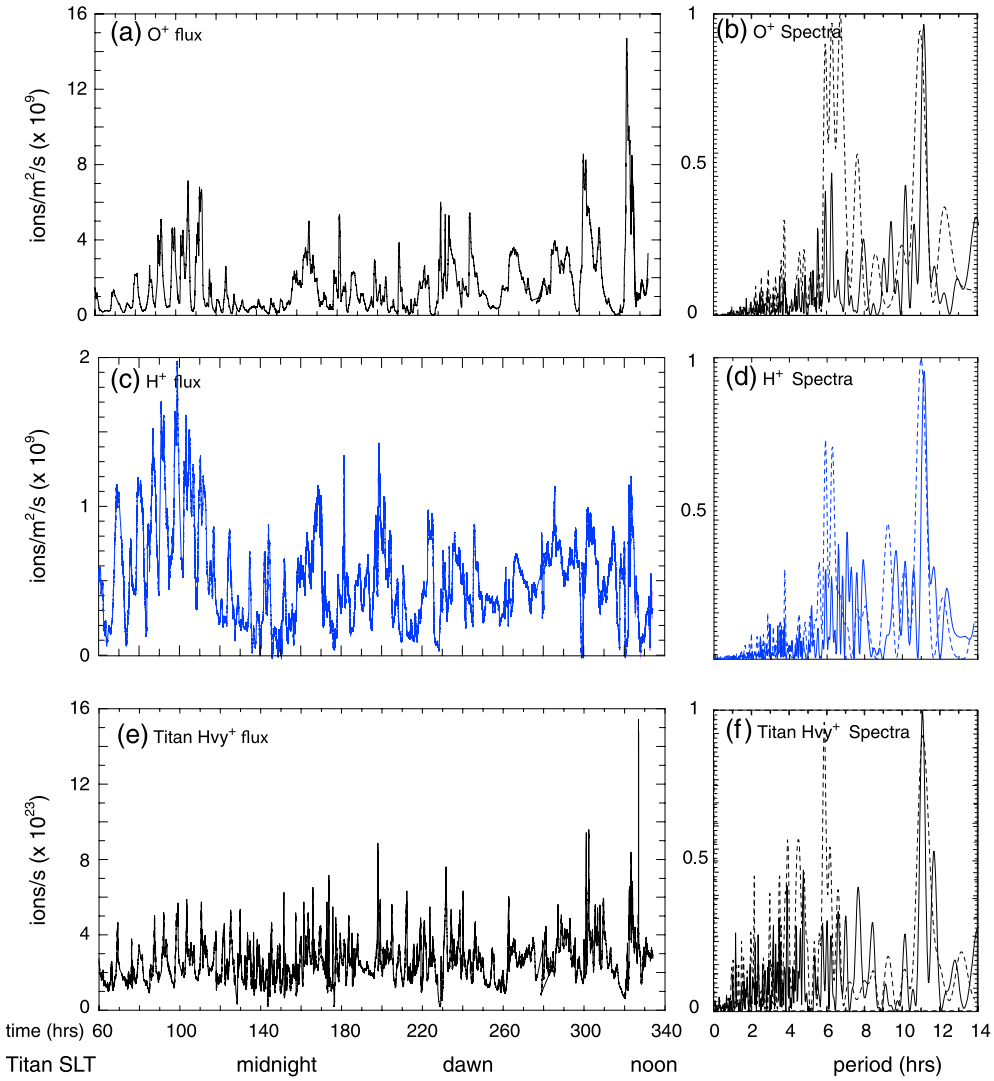

Figure 14. Left-hand side shows the calculated fluxes of O^+ and H^+ ions integrated over a 0.4 R_S cube about Titan and the corresponding total flux from Titan. The right-hand side shows the calculated spectrum derived from the full period (solid line) and between 60 and 240 h (dashed line). The O^+ flux from Saturn has a minimum between 120 and 160 h when Titan is near midnight and where it is most distant from the current sheet and the interchange fingers are weakest. Its spectrum has strong peaks at both the second harmonic and fundamental. The H^+ profile also has strong modulations with the dominant frequency at near the planetary period. The outflow from Titan shows modulations at both the second harmonic and fundamental, as well as higher frequency components which probably track the higher frequency components of the interchange fingers. The strength of the second harmonic appears to decline when the longer integration time is used.

of the magnetosphere. The results in the figure show that the southern hemisphere is subject to longer period perturbations than the northern hemisphere. This would be consistent with Titan producing more drag on the southern hemisphere than the northern hemisphere and damping out the high-frequency components.

[50] This difference in the time profiles is also seen in the spectra which are shown in Figures 15b and 15d. There are two peaks in the spectrum about the planetary period. For the southern hemisphere, the dominant peak is on the long side while the northern spectrum is peaked at the short period. This difference is consistent with the observations of *Gurnett et al*. [2009]. The main difference here is that the difference in the two periods is larger than reported by *Gurnett et al*. [2009]. This discrepancy may in part could be due to the fact that the model is only able to attain data over about 100 h, whereas the observations involve integrations over times scale nearly an order of magnitude longer. Some fine tuning of the assume plasma parameters may also refine the results. The important result here is not only that the model shows how the planetary period becomes embedded in the global magnetospheric dynamics and but that the response of the northern and southern hemispheres need not be identical with the winter hemisphere having the higher frequency/shorter period.

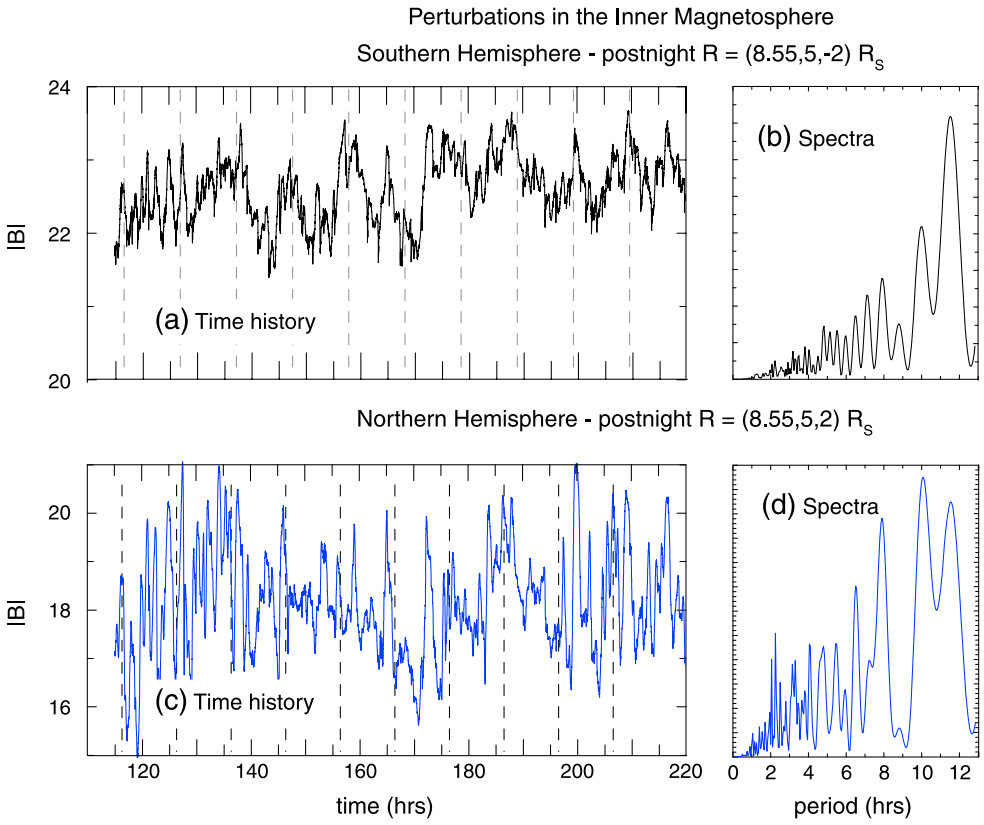

Figure 15. Time profile and spectra of the magnetic field at $R = (8.55,5,\pm 2)\ R_S$. The spectra are double peaked about the planetary period with the southern hemisphere having a stronger longer period component than the northern hemisphere. The latter has a much stronger high-frequency component and experiences less drag form Titan for southern solstice conditions.

6. Influence of Factors Controlling the Interchange Instability

[51] As noted in *Kidder et al.* [2009], the properties of the interchange instability are dependent on the solar wind conditions and the density of the Enceladus plasma torus. Thus, the expectation is that changing these parameters on long timescales will change the apparent fundamental frequency and that such changes could explain the apparent drift in the long-term periodicity of SKR. To demonstrate this effect, we increased the density of the Enceladus plasma torus by a factor of 4 at $t = 60$ h and repeated the simulations under identical solar wind conditions.

[52] The results for the inflow and outflow around Titan for this case are shown in Figure 16. These fluxes show modulation near the planetary period. However, examination of the inflowing spectra (Figures 16b and 16d) all shows that the fundamental period has shifted downward to about 9.6 h. Thus, while the density has been increased by a factor of 4, the frequency shift is small but discernible. This relatively weak dependence of the apparently frequency on the properties of the interchange instability could explain the small but significant change in the SKR period noted in section 1.

[53] The outflow from Titan (Figures 16e) shows a very strong local time enhancement between dawn and noon. The strength of this modulation is very much larger than in the nominal density case in Figure 14. This local time dependence is due the rebuilding of the interchange fingers as they rotate around the planet and their ability to reach Titan. Because of this local time effect, the spectra (Figure 16f) have strong components at both the fundamental and the planetary period embedded in its spectra.

[54] Figure 17 shows the magnetic perturbations and spectra for the same position in Figure 15 but for the present higher density cases. Again, very coherent perturbations are seen in the magnetic field data. The apparent frequency is decreased to 9.6 h, similar to the plasma fluxes in Figure 16. One important difference from the nominal density case is that there is not a significant difference apparent frequency of the northern and southern hemispheres. The change is most likely due to the weakened effect from drag produced by Titan (which density is fixed in the example) as the density of the interchange fingers is increased.

7. Comparisons With Cassini Rev 23 and 32

[55] In order to test the accuracy of the model, we compare the model results with Cassini magnetic field data from Rev 32 and 23, similar to *Jia et al.* [2012]. In Rev 32, Cassini is moving from about 30 R_S in X down the tail and 10 R_S in Y on the dawnside to a perigee of about $5R_S$, while in Rev 32, the spacecraft is moving from about 15 R_S on the nightside and 40 R_S on the dawnside to perigee. Because of the computational resources involved in running long duration

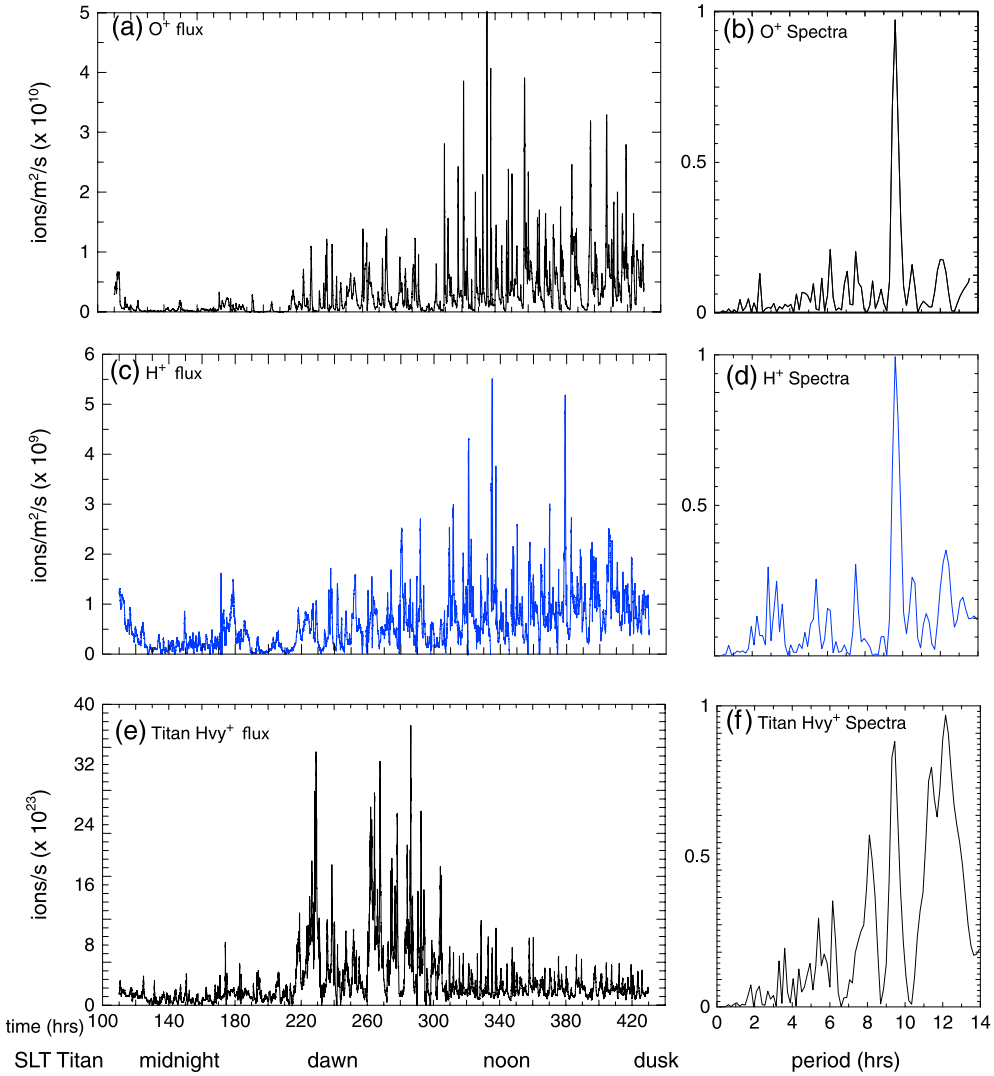

Figure 16. As in Figure 14, except that the density at the Enceladus torus has been increased by a factor of 4. Due to the increase in density, the apparent period of the system as seen from the inflowing ions decreases to 9.6 h.

simulations, we use the model data from section 5 that is save every 15–30 min and use a linear extrapolation in time and space to compare with the 1 min sample for the Cassini orbits. This extrapolation causes the loss of some of the higher frequency components but is sufficient to pick up the features of the fundamental and second harmonic components seen in the simulations.

[56] Figure 18 shows the comparison for Rev 32. Similar to *Jia et al*. [2012], we show the magnetic field with the Kronian dipole subtracted so that the perturbations can be more easily seen. The simulations show a magnitude that closely tracks the Cassini data for the bulk of the 100 h shown including the presence of several quasi-periodic oscillations. These oscillations are most notable in B_y and B_z, and the magnitudes of these perturbations seen within the model compare well with that seen in the data. It is important to note that our model also includes higher frequency components (albeit smoothed by the sampling). These same high-frequency components (particularly in comparison with the full simulations in Figures 15 and 17) are present in the Cassini observations. This result is very different from the results of *Jia et al*. [2012] where there is only one frequency component present by assumption.

[57] For the simulations, the model for the first 20 h places Cassini below the center of the current sheet (positive B_x), whereas the data indicate that it is above the plasma sheet with B_x negative. This discrepancy is most likely due to the fact that the actual solar wind conditions are not known, and we are using only nominal solar wind conditions for the entire duration of the simulations. A similar discrepancy is seen in the work of *Jia et al*. [2012].

[58] The results for Rev 23 are shown in Figure 19 using the same model data in Figure 18. It is seen that the model again does an excellent job in capturing the overall variations in the magnetic field for the 100 h shown. The model also captures the observed variations in the dominant components of B_x and B_y. The model though has the field lines slightly more vertical ($B_z < 0$) than observed by Cassini. An important feature of the model is that many of the observed and

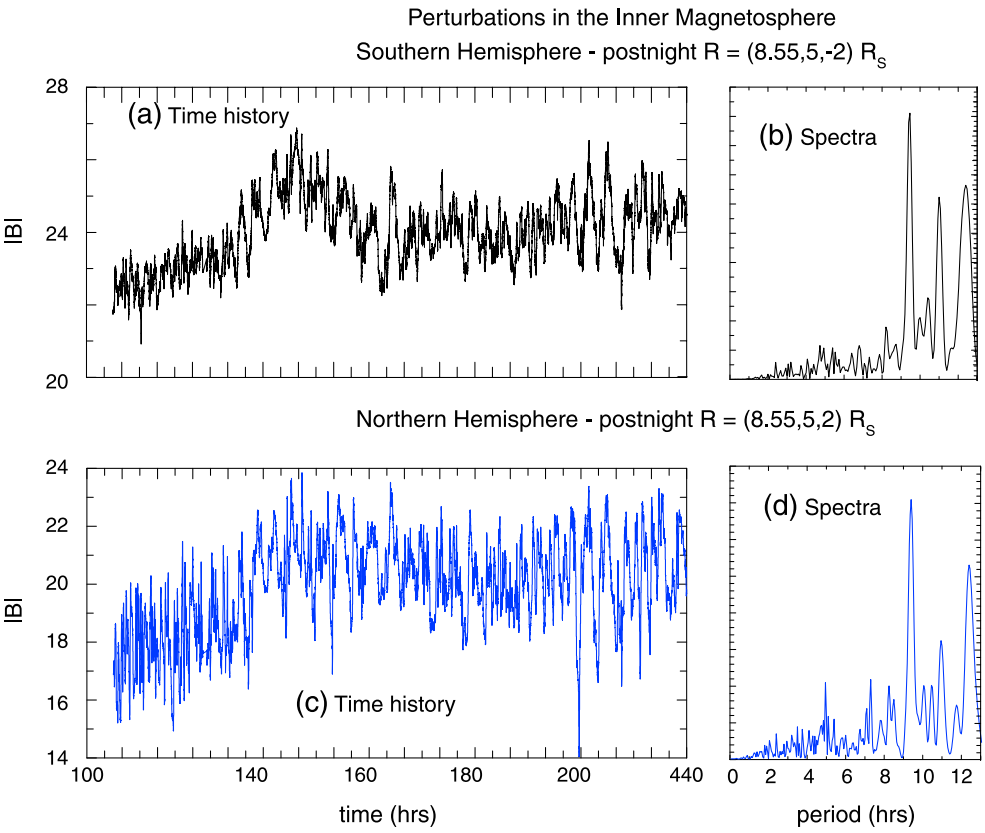

Figure 17. As in Figure 15, except that the density at the Enceladus torus has been increased by a factor of 4. Coherent oscillations are still evident in the magnetic field signature, though similar to the fluxes shown in Figure 16, the apparent frequency decreases to about 9.6 h, though there is still a component at the planetary rotation period.

model perturbations show very spikey features as opposed to the very sinusoidal features predicted by *Jia et al*. [2012].

[59] The fact that the model incorporates the higher frequency components and nonsinusoidal features of some of the periodicities suggests that the origin of the periodicities of the Kronian magnetosphere can be accounted for by the coupling of the interchange instability and Titan. The unspecified rotational features in the Kronian atmosphere of *Jia et al*. [2012] are not required.

8. Summary and Conclusions

[60] One of the outstanding problems for Saturn is determining why the rotation period appears in many of the plasma parameters when its magnetic field is aligned with the rotational axis. For such a configuration, a local observer does not expect to see a variation in the magnetic field, which is contrary to the observations which are reviewed in section 1. In this paper, the development of the interchange instability in the Kronian magnetosphere has been examined on sufficiently long timescales to determine whether the rotational period is indebted within the interchange fingers.

[61] The importance of interchange instability is that it is prevalent in much of the region where the periodicities are observed. Moreover, the interchange instability is driven by Saturn's rotation and therefore has rotational information embedded in it. The open question is what are the inherent frequencies embedded within the interchange fingers. Two different configurations were examined: (i) Saturn only simulations and (ii) Saturn/Titan simulations that use refinement grading to investigate the coupling between the Kronian magnetosphere and induced magnetosphere around Titan.

[62] In the Saturn only simulations, it is shown that there are typically five to seven interchange fingers present at any time and while a fixed observer will tend to see perturbations in both the magnetic field in the plasma parameters at the planet's rotational period, the large number of interchange fingers means that perturbations are seen at much shorter periods. This result is confirmed with a Fourier analysis of the time histories of the plasma parameters at fixed locations. The spectrum shows a strong peak that is near half the planetary period (i.e., second harmonic) with a weaker peak at the fundamental is present along with smaller peaks at some of the higher harmonics.

[63] For the Saturn/Titan simulations, the smaller interchange fingers are seen to be damped out, and there are typically only about three interchange fingers present. The reason for this partial stabilization is that the induced magnetosphere Titan produces a drag on the Kronian magnetosphere which can extend several R_S in radii toward Saturn and a few tens of R_S in the azimuthal direction around Saturn. Smaller interchange fingers are seen to be forced inside Titan's orbit producing a restriction of plasma flow, and conservation of flux and angular momentum causes the inner section of the interchange finger to speed up. Larger fingers can coalesce and some can be split by Titan's interaction.

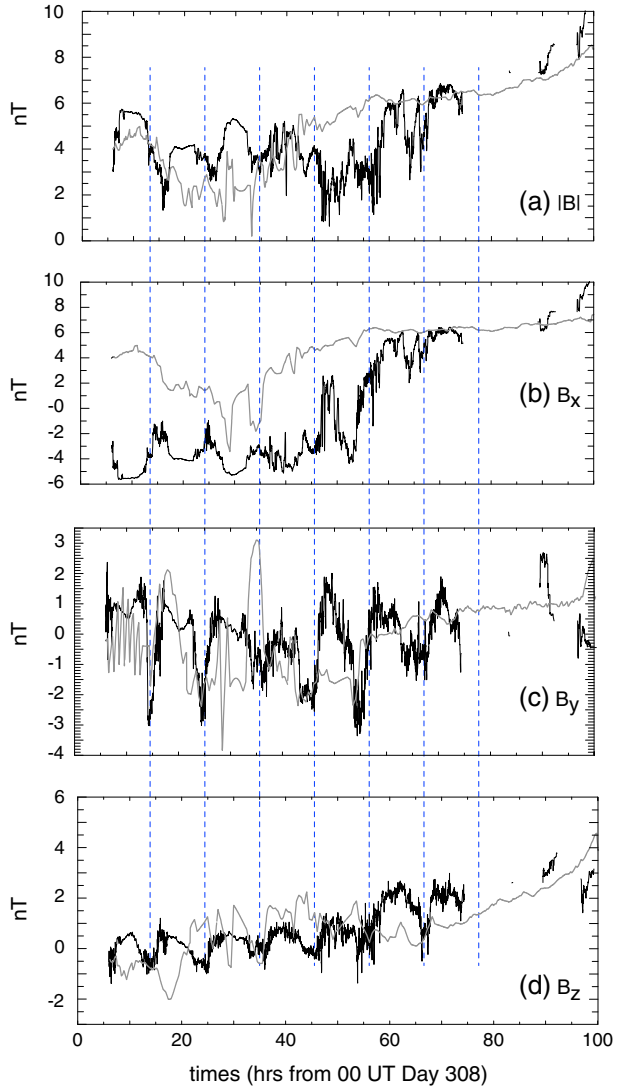

Figure 18. Comparison of the magnetic perturbations for Cassini Rev 32 (black lines) and the model results (gray lines) which uses data saved every 15 mins. The gray dashed lines indicate perturbations at the planetary period. The model results appear highly smoothed because it is based on 15 min time samples as opposed to continuously sampled data in Figures 14 and 16. Nevertheless, the model results have perturbations of similar magnitude and periodicity (including high-frequency components) to the Cassini data.

[64] As a result of the presence of fewer interchange fingers, the second harmonic features in the local magnetic field and plasma properties is weaker and a much stronger peak at the planetary rotation period develops. The modified interchange fingers are sufficiently large than they lead to an observable movement of the magnetopause which leads to reduction of density at high latitudes when the magnetosphere is expanding an increased density when it is contracting. In this way, an equatorial process can modify a high latitude process like SKR which favors low density and strong magnetic field regions.

[65] Moreover, the response of the northern and southern hemispheres need not be identical since Titan's position preferentially produces more drag on the hemisphere that it resides in. When the solar wind is incident on the southern hemisphere, Titan produces the strongest drag there and the period of modulation is longer in this hemisphere than in the southern hemisphere.

[66] Our model is similar to that of *Burch et al.* [2008] where the interchange instability is at the heart of creating the observed periodicities in the plasma and magnetic field properties. The main differences here are that the processes are not reconnection driven, and instead, it is Titan that has the dominant effect of removing the high-frequency components while acting on the interchange instability which requires plasma to be dominated by heavy ions in the inner magnetosphere and light ions in the outer magnetosphere of these fast rotating planets. It is this interaction which involves both magnetospheric/ionospheric and planetary/induced magnetosphere coupling that combine to set the dominant period to be near the planetary period. It is also important to note that the present model also incorporates the higher frequency

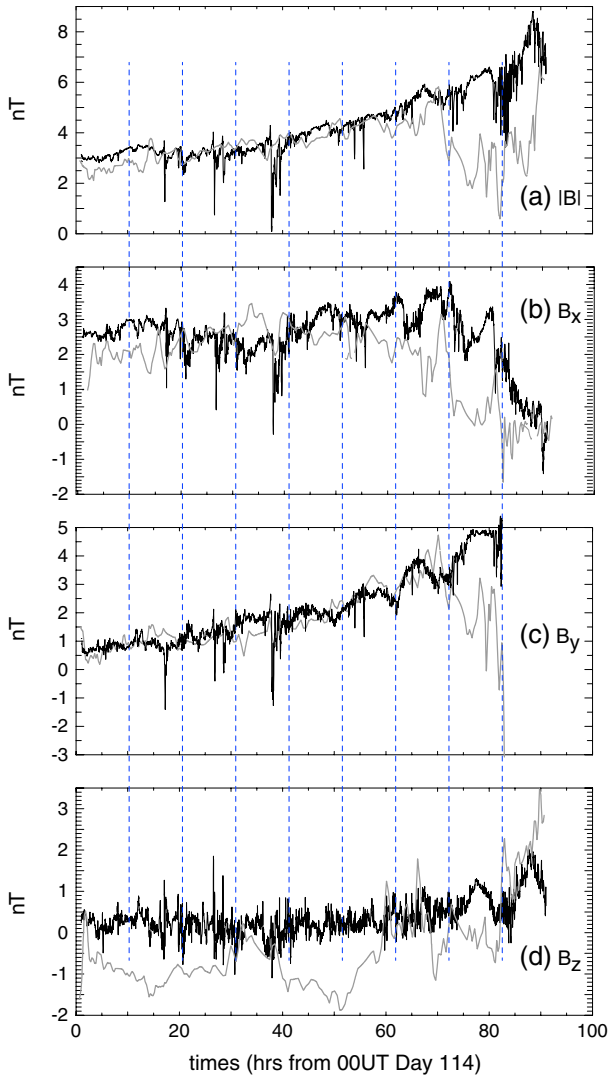

Figure 19. As in Figure 18, except for Cassini Rev 23. The model profiles closely match much of the Cassini observations, including spikey quasi-periodic perturbations as opposed to simple sinusoidal oscillations.

and nonsinusoidal features that are present in the Cassini magnetic field observations.

[67] It is also important to note that the model does not require the assumption of any confined ionospheric sources as proposed in alternate models. There is also the suggestion that additional longer periods processes are occurring within the magnetosphere for which we have not been able to examine in the present paper and longer simulations have to be undertaken. Further work needs to evaluate seasonal effects where Titan's position relative to the center of the plasma sheet changes. Such effects affect the asymmetry between the northern and southern periodicities. Effects from long duration solar wind conditions also have the potential for modifying the interchange instability and hence the apparent period of the Kronian system.

[68] **Acknowledgments.** This work was supported by NASA grant to the University of Washington and to the Georgia Institute of Technology.

[69] Masaki Fujimoto thanks the reviewers for their assistance in evaluating this paper.

References

Burch, J. L., J. Goldstein, P. Mokashi, W. S. Lewis, C. Paty, D. T. Young, A. J. Coates, M. K. Dougherty, and N. André (2008), On the cause of Saturn's plasma periodicity, *Geophys. Res. Lett.*, *35*, L14105, doi:10.1029/2008GL034951.

Carbary, J. F., D. G. Mitchell, S. M. Krimigis, D. C. Hamilton, and N. Krupp (2007), Charged particle periodicities in Saturn's outer magnetosphere, *J. Geophys. Res.*, *112*, A06246, doi:10.1029/2007JA012351.

Carbary, J. F., D. G. Mitchell, P. Brandt, E. C. Roelof, and S. M. Krimigis (2008), Periodic tilting of Saturn's plasma sheet, *Geophys. Res. Lett.*, *35*, L24101, doi:10.1029/2008GL036339.

Carbary, J. F., D. G. Mitchell, S. M. Krimigis, and N. Krupp (2009), Dual periodicities in energetic electrons at Saturn, *Geophys. Res. Lett.*, *36*, L20103, doi:10.1029/2009GL040517.

Clarke, K. E., D. J. Andrews, C. S. Arridge, A. J. Coates, and S. W. H. Cowley (2010), Magnetopause oscillations near the planetary period at Saturn: Occurrence, phase, and amplitude, *J. Geophys. Res.*, *115*, A08209, doi:10.1029/2009JA014745.

Desch, M. D., and M. L. Kaiser (1981), Voyager measurements of the rotation period of Saturn's magnetic field, *Geophys. Res. Lett.*, *8*, 253–256, doi:10.1029/GL008i003p00253.

Espinosa, S. A., and M. K. Dougherty (2000), Periodic perturbations in Saturn's magnetic field, *Geophys. Res. Lett.*, *27*, 2785–2788, doi:10.1029/2000GL000048.

Espinosa, S. A., D. J. Southwood, and M. K. Dougherty (2003), Reanalysis of Saturn's magnetospheric field data view of spin-periodic perturbations, *J. Geophys. Res.*, *108*(A2), 1085, doi:10.1029/2001JA005083.

Giampieri, G., M. K. Dougherty, E. J. Smith, and C. T. Russell (2006), A regular period of Saturn's magnetic field that may track its internal rotation, *Nature*, *441*, 62–64, doi:10.1038/nature/04750.

Gurnett, D. A., et al. (2005), Radio and plasma wave observations at Saturn from Cassini's approach and first orbit, *Science*, *307*, 1255–1259, doi:10.1126/science.1105356.

Gurnett, D. A., A. M. Persoon, W. S. Kurth, J. B. Groene, T. F. Averkamp, M. K. Dougherty, and D. J. Southwood (2007), The variable rotation period of the inner region of Saturn's plasma disk, *Science*, *316*, 442–445, doi:10.1126/science.1138562.

Gurnett, D. A., A. Lecacheux, W. S. Kurth, A. M. Persoon, J. B. Groene, L. Lamy, P. Zarka, and J. F. Carbary (2009), Discovery of a north–south asymmetry in Saturn's radio rotation period, *Geophys. Res. Lett.*, *36*, L16102, doi:10.1029/2009GL039621.

Jackman, C. M., and C. S. Arridge (2011), Statistical properties of the magnetic field in the Kronian magnetotail lobes and current sheet, *J. Geophys. Res.*, *116*, A05224, doi:10.1029/2010JA015973.

Jia, X., and M. G. Kivelson (2012), Driving Saturn's magnetospheric periodicities from the upper atmosphere/ionosphere: Magnetotail response to dual sources, *J. Geophys. Res.*, *117*, A11219, doi:10.1029/2012JA018183.

Jia, X., M. G. Kivelson, and T. I. Gombosi (2012), Driving Saturn's magnetospheric periodicities from the upper atmosphere/ionosphere, *J. Geophys. Res.*, *117*, A04215, doi:10.1029/2011JA017367.

Kellett, S., C. S. Arridge, E. J. Bunce, A. J. Coates, S. W. H. Cowley, M. K. Dougherty, A. M. Persoon, N. Sergis, and R. J. Wilson (2010), Nature of the ring current in Saturn's dayside magnetosphere, *J. Geophys. Res.*, *115*, A08201, doi:10.1029/2009JA015146.

Kidder, A., R. M. Winglee, and E. M. Harnett (2009), Regulation of the centrifugal interchange cycle in Saturn's inner magnetosphere, *J. Geophys. Res.*, *114*, A02205, doi:10.1029/2008JA013100.

Kivelson, M. G., and D. J. Southwood (2005), Dynamical consequences of two modes of centrifugal instability in Jupiter's outer magnetosphere, *J. Geophys. Res.*, *110*, A12209, doi:10.1029/2005JA011176.

Kurth, W. S., T. F. Averkamp, D. A. Gurnett, J. B. Groene, and A. Lecacheux (2008), An update to a Saturnian longitude system based on kilometric radio emissions, *J. Geophys. Res.*, *113*, A05222, doi:10.1029/2007JA012861.

Menietti, J. D., P. H. Yoon, and D. A. Gurnett (2007), Possible eigenmode trapping in density enhancements in Saturn's inner magnetosphere, *Geophys. Res. Lett.*, *34*, L04103, doi:10.1029/2006GL028647.

Paranicas, C., D. G. Mitchell, E. C. Roelof, P. C. Brandt, D. J. Williams, S. M. Krimigis, and B. H. Mauk (2005), Periodic intensity variations in global ENA images of Saturn, *Geophys. Res. Lett.*, *32*, L21101, doi:10.1029/2005GL023656.

Snowden, D., R. M. Winglee, and A. Kidder (2011a), Titan at the Edge I: Titan's interaction with Saturn's magnetosphere in the pre-noon sector, *J. Geophys. Res.*, *116*, A08229, doi:10.1029/2011JA016435.

Snowden, D., R. M. Winglee, and A. Kidder (2011b), Titan at the Edge II: A global simulation of Titan exiting and re-entering Saturn's magnetosphere at 13.6 SLT, *J. Geophys. Res.*, *116*, A08230, doi:10.1029/2011JA016436.

Winglee, R. M., D. Snowden, and A. Kidder (2009), Modification of Titan's ion tail and the Kronian magnetosphere: Coupled magnetospheric simulations, *J. Geophys. Res.*, *114*, A05215, doi:10.1029/2008JA013343.